AFM tips

# Preventing Nanoscale Wear of Atomic Force Microscopy Tips Through the Use of Monolithic Ultrananocrystalline Diamond Probes

*J. Liu, D. S. Grierson, N. Moldovan, J. Notbohm, S. Li, P. Jaroenapibal, S. D. O'Connor, A. V. Sumant, N. Neelakantan, J. A. Carlisle, K. T. Turner,* and R. W. Carpick**

*Nanoscale wear is a key limitation of conventional atomic force microscopy (AFM) probes that results in decreased resolution, accuracy, and reproducibility in probe-based imaging, writing, measurement, and nanomanufacturing applications. Diamond is potentially an ideal probe material due to its unrivaled hardness and stiffness, its low friction and wear, and its chemical inertness. However, the manufacture of monolithic diamond probes with consistently shaped small-radius tips has not been previously achieved. The first wafer-level fabrication of monolithic ultrananocrystalline diamond (UNCD) probes with <5-nm grain sizes and smooth tips with radii of 30–40 nm is reported, which are obtained through a combination of microfabrication and hot-filament chemical vapor deposition. Their nanoscale wear resistance under contact-mode scanning conditions is compared with that of conventional silicon nitride ($SiN_x$) probes of similar geometry at two different relative humidity levels (≈15 and ≈70%). While $SiN_x$ probes exhibit significant wear that further increases with humidity, UNCD probes show little measurable wear. The only significant degradation of the UNCD probes observed in one case is associated with removal of the initial seed layer of the UNCD film. The results show the potential of a new material for AFM probes and demonstrate a systematic approach to studying wear at the nanoscale.*

**Keywords:**
- atomic force microscopy
- diamond
- mechanical properties
- nanocrystalline materials
- tribology

[*] Prof. K. T. Turner, J. Liu, Dr. D. S. Grierson, J. Notbohm,[+] Dr. S. Li,[†] S. D. O'Connor
University of Wisconsin–Madison
Madison, WI 53706 (USA)
E-mail: kturner@engr.wisc.edu

Prof. R. W. Carpick, Dr. P. Jaroenapibal[‡]
University of Pennsylvania
Philadelphia, PA 19104 (USA)
E-mail: carpick@seas.upenn.edu

Dr. N. Moldovan, N. Neelakantan, Dr. J. A. Carlisle
Advanced Diamond Technologies
Romeoville, IL 60446 (USA)

Dr. A. V. Sumant
Center for Nanoscale Materials
Argonne National Laboratory
Argonne, IL 60439 (USA)

[+] Current address:
California Institute of Technology
Pasadena, CA (USA)

[†] Current address:
nLight
Vancouver, WA (USA)

[‡] Current address:
Industrial Engineering Department
Khon Kaen University (Thailand)

DOI: 10.1002/smll.200901673

 WILEY InterScience DISCOVER SOMETHING GREAT

© 2010 Wiley-VCH Verlag GmbH & Co. KGaA, Weinheim

## 1. Introduction

Atomic force microscopy (AFM) is an indispensable tool for nanotechnology with continually expanding applications including atomic-scale imaging, metrology, and property measurements,[1,2] as well as nanomanufacturing applications such as nanolithography[3,4] and high-density data storage.[5] However, the wear of AFM probes is a serious limitation.[6–15] As AFM techniques advance from use in research laboratories to industrial applications, the tips' performance and stability becomes more critical. The ideal probe tips should be sharp ($<$10 nm radius), resistant to wear and contamination for long periods of use, and chemically stable. Nanoscale sharpness has long been achieved through the use of etched-silicon[16] or carbon-nanotube[17,18] probes. However, the remaining requirements are far more challenging and are not addressed by the current state of the art. One reason for this is that wear of materials involves a complex set of phenomena, and fundamental understanding is lacking. In fact, nanoscale studies of wear enabled by AFM have the potential to provide important insights into the fundamental mechanisms of wear, thus resulting in a better understanding of this technologically important phenomenon that controls the failure of systems from car engines to microengines,[19] with substantial economic, energetic, and environmental impacts.[20]

Silicon (Si) and silicon nitride ($SiN_x$) are the most common tip materials, but have modest mechanical properties (see Table 1). Single-crystal Si tips are prone to fail via brittle fracture and have naturally hydrophilic oxidized surfaces, which have high adhesion and are susceptible to environmentally accelerated degradation.[21,22] $SiN_x$ has higher hardness and macroscopic wear resistance than Si and thus is frequently used as a protective layer or as an alternative to Si tips to reduce wear.[23,24] However, $SiN_x$ tips can still experience substantial wear during normal use. In the nanoscale tip–sample contact, stresses induced by surface adhesive forces alone can exceed the strength of Si-based tip materials.[15,25] Diamond has long been considered the ideal AFM probe material due to its unrivaled bulk stiffness and strength, its low adhesion and friction under many conditions, and its chemical inertness.

Early diamond probes were made by fracturing, grinding, or polishing bulk diamond at high cost and with limited reproducibility.[26,27] Attaching sharp single-crystal diamond tips of $\approx$10 nm radius to cantilevers by using glue has also been reported.[28] However, the serial process for making these tips is not scalable and the thermal stability of the glue can be problematic. Carbon-nanotube tips have high mechanical robustness, extremely high aspect ratios, and small diameters.[18,29,30] However, tube buckling and detachment limit the range of applied forces. Hence their application to nanomachining or mechanical probing is not widespread.

Diamond films have been coated on existing Si or tungsten tips for wear resistance, but such tips often suffer from coating delamination, irregular and nonreproducible tip shapes, and fracture along weak grain boundaries in the polycrystalline diamond films.[15,31,32] Microfabrication of monolithic diamond probes using a molding technique, in which diamond films are deposited into sacrificial silicon molds, can provide better control over the tips' size and roughness.[31,33] Unfortunately, the grain size of conventional microcrystalline diamond (MCD) and even nanocrystalline diamond (NCD) limits the achievable quality of the tip, and polycrystalline diamond films tend to have inferior mechanical properties to single-crystal diamond.[34] Smaller grain sizes (2–5 nm) and better mechanical properties can be obtained with ultrananocrystalline diamond (UNCD).[35] The first UNCD molded probes, grown using microwave plasma chemical vapor deposition (MPCVD), showed improved wear resistance.[36,37] These UNCD tips were rough with large overall sizes ($\approx$100 nm), and the tip apex was typically composed of randomly positioned grain clusters of radii $\approx$15 nm, due to the difficulties in the mold-filling process. Tip degradation via fracture was observed during wear testing.

Herein, we report the wafer-level fabrication of monolithic UNCD probes grown by hot-filament chemical vapor deposition (HFCVD) with consistently small ($<$40 nm) smooth tips, and dramatically less wear than conventional $SiN_x$ probes under harsh scan conditions at 15 and 70% relative humidity (RH). $SiN_x$ probes are chosen for comparison due to their popularity for contact-mode AFM applications, and because they are fabricated using a molding process very similar to the method used here for UNCD. Therefore, the initial geometries being compared are similar.

## 2. Results and Discussion

### 2.1. Filling the Mold with UNCD

The fabrication scheme used here is based on the mold-filling method commonly used to produce monolithic $SiN_x$ probes;[31] details are provided in the Experimental Section. Consistent filling of the pyramidal Si molds with diamond is challenging and normally a "seeding" process is needed to nucleate the film growth. Standard seeding utilizing detonation nanodiamond particles[38] yields smooth and high-quality UNCD films on flat, unstructured silicon surfaces, but results

**Table 1.** Comparison of the properties of silicon, $SiN_x$, single-crystal diamond, and UNCD. Friction data are from the same set of experiments, and were measured at room temperature at 3.4 Torr $O_2$, except for silicon nitride and UNCD which were measured in air and humid air, respectively.

| Property | Single-crystal Si | $SiN_x$ | Single-crystal diamond | UNCD |
|---|---|---|---|---|
| Young's modulus [GPa] | 130–180 | 150–250 | 1100 | 980 |
| Hardness [GPa] | 5.4 | 16 | 100 | 98 |
| Fracture toughness [MPa $m^{1/2}$] | 1 | 3–6 | 5–14 | 4.7–7.2 |
| Macroscopic friction coefficient | 0.6 | 0.15–0.32 | 0.01–0.02 | 0.02–0.03 (humid air) |
| Macroscopic wear rate [$mm^3\ N^{-1}\ m^{-1}$] | $10^{-3}$–$10^{-4}$ | $10^{-4}$–$10^{-6}$ | $\approx 10^{-7}$ | $\approx 10^{-8}$ |
| References | [21,65] | [21,65] | [21] | [52,64] |


© 2010 Wiley-VCH Verlag GmbH & Co. KGaA, Weinheim

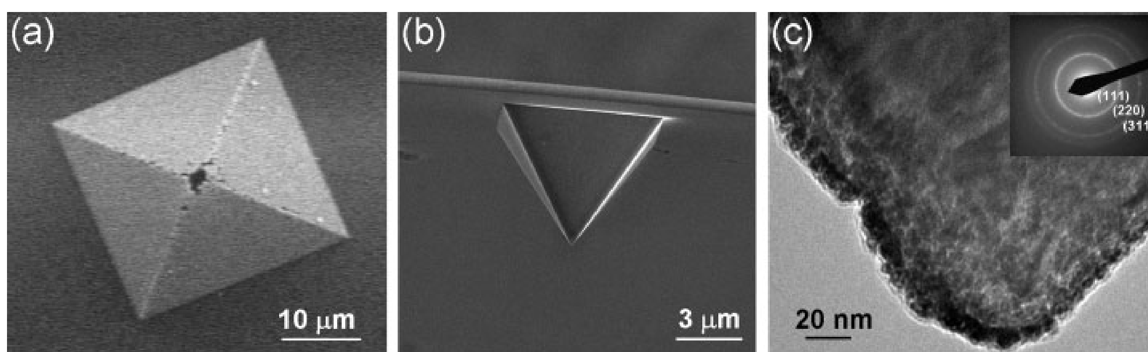


Figure 1. a) Top-view SEM image of a defective UNCD tip grown without nucleation enhancement. b) Side-view SEM image of a UNCD tip grown with nucleation enhancement. c) Typical TEM image of a UNCD tip with nucleation enhancement, used in this experiment. Inset: the corresponding SAD pattern, in which the reciprocal lattice spacing matches that of a diamond structure.

in incomplete filling at a three-dimensional mold with nanoscale tip (Figure 1a). Depositing a thin tungsten layer prior to seeding with nanodiamond particles greatly enhances the initial nucleation density.[36,39] The use of such a layer in addition to more highly dispersed suspensions of nanodiamond particles (known as ultradispersed diamond or UDD) and HFCVD produces tips with apices that are fully dense. Scanning electron microscopy (SEM) and transmission electron microscopy (TEM) images of typical as-fabricated UNCD tips are shown in Figure 1b and c, respectively. In the bright-field TEM image (Figure 1c), the brighter lines close to the tip apex indicate the grain boundaries, which consist of $sp^2$- and $sp^3$-bonded carbon. Multiple grains less than 5 nm in diameter are resolved. The selected-area diffraction (SAD) pattern in the inset in Figure 1c reveals the polycrystalline diffraction rings of the diamond structure and confirms the presence of the UNCD structure at the tip. A darker layer of diamond grains encompassing the tip body is also observed. Given that no other diffraction was observed in the SAD pattern, this darker layer is believed to be the NCD seeding layer that remains on the tip in some cases after fabrication.

## 2.2. Wear Performance of UNCD and $SiN_x$ Tips

The mechanisms that govern tip wear in AFM are not well understood. Atomic-scale wear models are still being developed, and thus direct experimental measurements are needed to assess the performance of tips and to validate models.[10,40] To evaluate the stability and reliability of AFM tips, researchers have performed wear tests with different tip and sample materials under a variety of conditions.[23,32,41–45] However, a standardized evaluation protocol to accurately and reproducibly monitor nanoscale wear of AFM tips does not exist. Recent experimental work,[41] for example, measures tip wear for long scan distances (meters) and demonstrates that atom-by-atom attrition is observed for Si AFM tips sliding against a polymer. Herein, the wear behavior of commercial $SiN_x$ and the fabricated UNCD tips, sliding against UNCD test samples, was examined by a quantitative protocol that involved sliding each tip nominally 204.8 mm using contact-mode raster scanning (corresponding to $200, 1 \times 1\ \mu m^2$ AFM images in which the nominal scan distance is 1.024 mm in the image) under two humidity levels. The tips are loaded by adhesive forces alone in the first half of each test (images 1–100), and with an additional external compressive load equal to twice the pull-off force during scanning in the second half of each test (images 101–200). The tips are characterized over the course of the wear test by using TEM, blind tip reconstruction (BTR), and pull-off force measurements. The protocol is described in detail in the Experimental Section; its key unique feature is the combined use of direct (TEM) and indirect (BTR and pull-off force measurements) evaluation of the tip throughout the wear test.

### 2.2.1. AFM Images

A topographic AFM image represents a convolution of both the actual sample features and the geometry of the tip that imaged them.[46] Figure 2 shows topographic AFM images of a UNCD sample acquired by two UNCD and two $SiN_x$ tips over the course of wear tests for each tip. The tests were conducted in a nitrogen environment at 15 and 70% RH, respectively. The full scale of the axes in the $x$, $y$, and $z$ directions of the three-dimensional images are $1\ \mu m \times 1\ \mu m \times 100\ nm$, respectively. The images acquired by the UNCD tips for both RH levels (Figure 2a–c and d–f, respectively) have an almost constant range of $z$ heights and features with constant in-plane dimensions (as evaluated qualitatively by examining the size of the in-plane features). Some evidence of tip artifacts (feature doubling) is seen in Figure 2c and f, but the observed features remain sharp.

In contrast, the topography images obtained by $SiN_x$ tips show gradual reduction in the $z$-height data range, and strong to severe broadening of the in-plane dimensions of the features for the two humidity levels (Figure 2g–i and j–l, respectively). The convolution of the true sample topography and the tip shape becomes more noticeable as the tip's size exceeds the typical size of the features on the sample. Correspondingly, instead of exhibiting the small, randomly oriented features characteristic of UNCD surfaces, the AFM images obtained using severely worn and flattened $SiN_x$ tips (e.g., Figure 2i,l) repeatedly contain large, smooth features. This decrease in lateral resolution is much more severe for images acquired after longer scanning distances (images 100 to 200). Also, results from the high-humidity test show a much faster loss of image


© 2010 Wiley-VCH Verlag GmbH & Co. KGaA, Weinheim

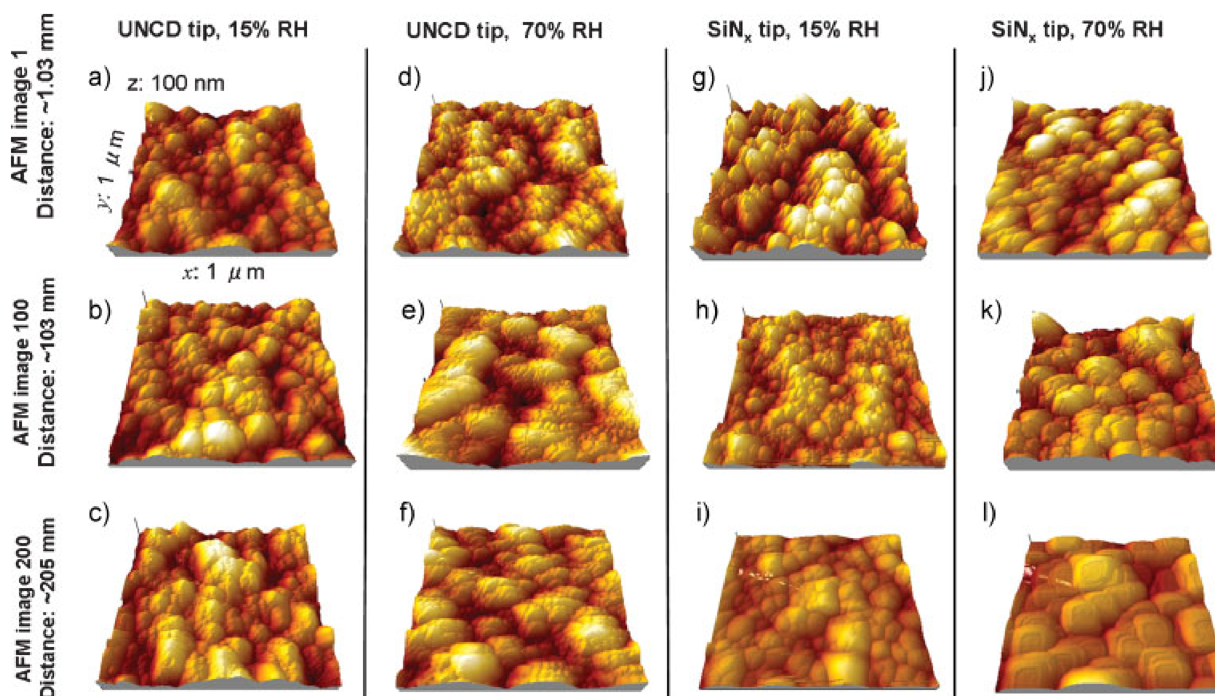


**Figure 2.** a–c) AFM topographic scans ($1 \times 1\ \mu m^2$) of a UNCD sample imaged by a UNCD tip at 15% RH after completing 1, 100, and 200 contact-mode images. d–f) UNCD sample imaged by a different UNCD tip at 70% RH after completing 1, 100, and 200 contact-mode images. g–i) and j–l) UNCD sample imaged by two commercial $SiN_x$ tips at ≈15 and ≈70% RH, respectively. Each AFM image was acquired at a different location on the sample. The full color scale of the *z* axis for all images is 100 nm. There is ±5% uncertainty in the scan distances.

resolution for the $SiN_x$ tip (Figure 2j–l) compared with the low-humidity test (Figure 2g–i). This accelerated wear phenomenon at higher humidity could be attributed to the interaction of water molecules with the native $SiO_x$, which lowers the energy barrier for atoms to be removed from the tip.[47–49] By the 200th image (Figure 2l), the $SiN_x$ tip completely failed to resolve any sample features. Instead, the multiple square-shaped protrusions in the topography image are essentially images of the flattened tip.

### 2.2.2. Tip Geometries

The evolution of tip geometries throughout the wear tests is directly characterized by TEM at periodic intervals (Figure 3). In agreement with the AFM images showing constant resolution, no substantial changes in overall geometry or tip radius were observed for the UNCD tips tested at both humidity levels over the entire wear test (Figure 3a–f), except for a subtle change shown in the inset of Figure 3d, which will be discussed further below. The $SiN_x$ tips, however, shown in the corresponding TEM images experience significant wear and blunting after 100 AFM scans (≈100 mm scan distance; loaded by adhesive forces only), and more severe wear from scan 101 to 200 under the additional external load (Figure 3g–l). The $SiN_x$ tip exhibits significantly more wear at high humidity (70% RH), which indicates a wear behavior that depends strongly on environment. A large portion of the $SiN_x$ tip was removed and the apex of the tip was flattened (Figure 3k,l). This correlates with the multiple square features observed in the corresponding AFM images (Figure 2l). Contamination near the $SiN_x$ tip apex was also observed (Figure 3h,i), which may be due to fracture and reattachment of material from the tip. The TEM images were overlaid to illustrate the evolution of the AFM tips over the course of the wear test (Figure 4), which immediately demonstrates the gradual and progressive wear of the $SiN_x$ tips, and little to no observable wear of the UNCD tips as the overlays are not easily distinguished from one another.

Figure 4b and the inset in Figure 3d show that a layer (<20 nm in thickness) appears to peel off from the end of the UNCD tip after 50 scans. This layer, which appears darker than the bulk tip, is also visible in the higher-resolution TEM image in Figure 1c, as well as the sidewalls of the tip in Figure 3a–c, and is believed to be the diamond-nanoparticle seed layer used to nucleate the UNCD growth. The structural integrity of the interface between the seed layer and bulk UNCD could be weak and thus subject to interfacial fracture and delamination; the mechanical properties of this interface have never been studied previously. Most importantly, after the loss of the seeding layer, demonstrated in the subsequent TEM images (Figure 3e,f), the underlying UNCD is stable and exhibits no measurable geometric change at high humidity, even under the higher external load. Note that the UNCD tip tested at low humidity (15% RH) also has the darker-contrast seed layer attached to the sidewalls of the tip, but not at the tip apex that is in contact with the sample surface during sliding (Figure 1a–c); this indicates that the seed layer was initially missing from this tip.

Abbreviated wear tests were conducted on six additional UNCD tips by acquiring either 100 or 200 images at zero applied load at humidity levels ranging from 30 to 70% RH. Three of these tips were unsharpened UNCD probes (one of which was lightly doped with boron), and three others were from a batch of probes made using oxide-sharpened molds. For the sharpened probes, we were unable to determine whether or

 © 2010 Wiley-VCH Verlag GmbH & Co. KGaA, Weinheim 

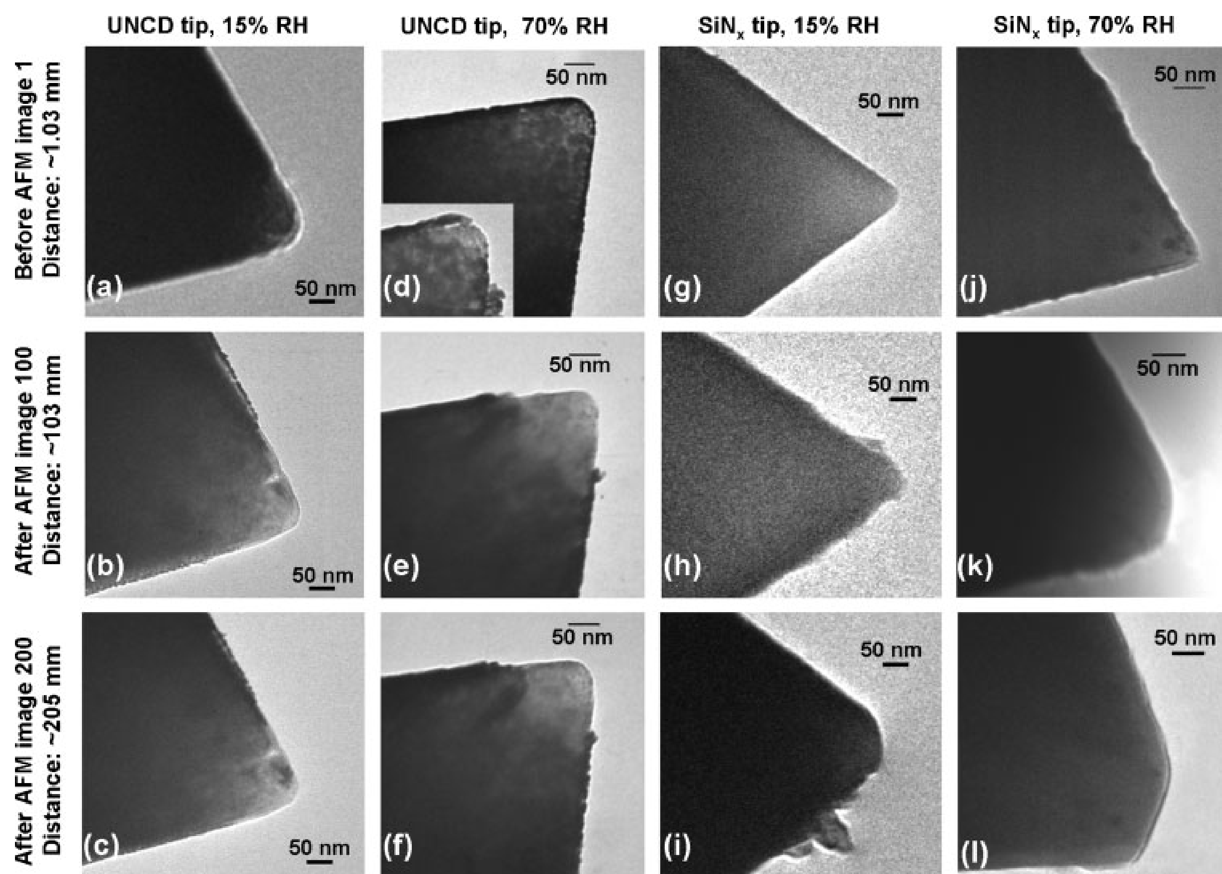


**Figure 3.** a–c) TEM images of a UNCD tip before any AFM imaging (a), and after completing 100 (b) and 200 (c) contact-mode $1 \times 1\ \mu m^2$ images on a UNCD sample at $\approx$15% RH. d–f) Similarly, TEM images of a UNCD tip before AFM imaging and after completing 100 and 200 images at $\approx$70% RH. The inset in (d) is the TEM image of the tip after 50 AFM images were recorded. g–i) and j–l) TEM images of commercial SiN$_x$ tips before AFM imaging and after completing 100 and 200 UNCD images at 15 and 70% RH, respectively. There is $\pm$5% uncertainty in the scan distances.

not the material at the end of the tip truly consisted of UNCD, as the TEM images were ambiguous. However, in all these tests, consistent results were obtained: wear was substantially lower than that for the SiN$_x$ tips. For the unsharpened probes, delamination of the seed layer was not observed in two cases; in the third case the seed layer had already delaminated at the end of the tip before any scanning took place. There is no clear correlation between scanning-induced seed layer delamination and humidity in these measurements. The results are also consistent with a recent study that compared UNCD with SiN$_x$ tips.[50]

### 2.2.3. Quantifying Adhesion and Nanoscale Tip Wear

To quantify the changes in tip geometry and the corresponding volume loss, tip profiles were quantitatively extracted from the TEM images (Figure 5). Furthermore, a BTR algorithm was used to estimate the tip profile from the AFM topography images themselves based on a convolution/deconvolution algorithm (details are provided in the Experimental Section). In Figure 5a, c, and d, the tip profiles obtained by BTR and TEM illustrate very good agreement. However, in the comparison of profiles in Figure 5b (for a UNCD tip before scanning at 70% RH), BTR produces a sharper tip profile than the TEM observation. This may be due to the fact that the BTR only captures a small portion of the tip that is in contact with the sample, and thus the reconstructed tip might only represent a small protrusion from the UNCD tip that is in contact with the sample. Overall, while TEM reveals global, broad changes in tip geometry relative to the unworn region of the tip, BTR allows local tip-shape quantification continuously throughout the wear test without having to remove the probe from the AFM instrument.

The tip radii deduced from TEM and BTR as a function of sliding distance (Figure 6a) agree with each other and show a similar trend in that UNCD tips exhibit a nearly constant radius, and SiN$_x$ tips exhibit an overall increase in tip radius. In particular, a jump in the slope of the curves for SiN$_x$ tips is obvious between the first and second 100 images where the total load was tripled, as well as between 15 and 70% RH where the humidity was increased. Applied load has a considerable influence on macroscopic wear due to increased contact stresses that promote bond breaking and fracture. The presence of water molecules tends to make bond rupture of the oxidized layer on the surface of the SiN$_x$ tip easier, and thus leads to increased wear according to macroscopic[47–49] and nanoscopic studies.[9] Maw et al. observed that in aqueous solutions, the wear of a SiN$_x$ tip is promoted by surfaces exhibiting hydroxide terminations.[9] They propose that transient chemical bonds across the interface, which involve hydroxyl groups that deprotonate to form Si–O–Si linkages, are stimulated by


© 2010 Wiley-VCH Verlag GmbH & Co. KGaA, Weinheim

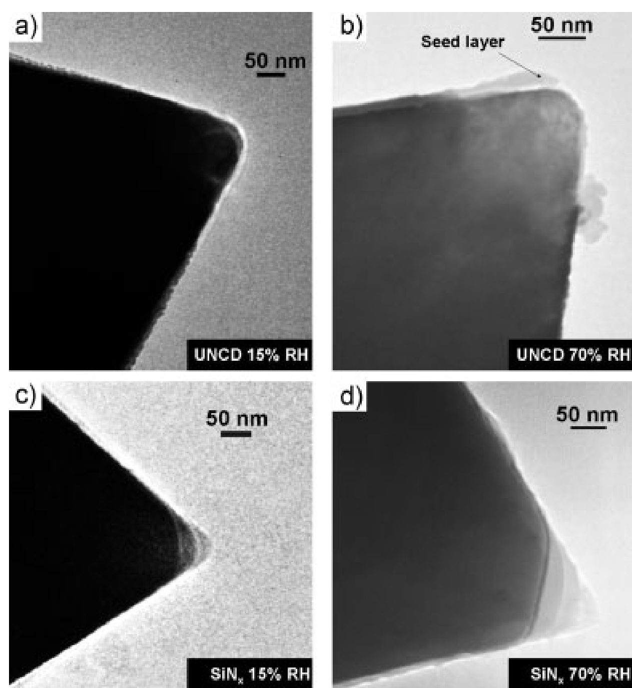


Figure 4. a) Overlaid TEM images of a UNCD tip before, after 100, and after 200 AFM images at 15% RH. The identical shapes prevent one from discerning any significant differences. b) Overlaid TEM images of a UNCD tip before, after 100, and after 200 AFM images at 70% RH, which shows the delamination of the UNCD seeding layer. c,d) Similarly, overlaid TEM images of a $SiN_x$ tip showing wear at 15 and 70% RH, respectively.

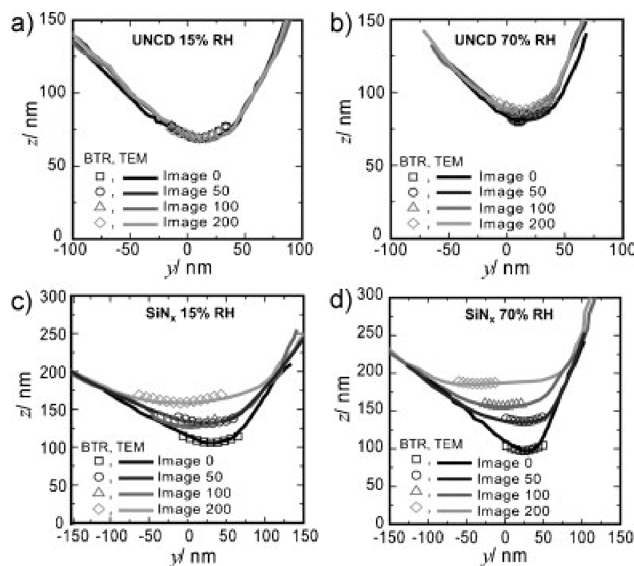


Figure 5. a,b) Overlaid two-dimensional tip profiles extracted from TEM (solid lines) and BTR (symbols) of the UNCD tips after acquiring 0, 50, 100, and 200 AFM images at 15 and 70% RH, respectively. c,d) Overlaid two-dimensional tip profiles of the commercial $SiN_x$ tips by TEM and from BTR methods at 15 and 70% RH, respectively.

the applied stresses. These siloxane bridges eventually rupture in processes that can lead to the removal of atoms from the tip. Carbon surfaces were not considered in that study, but it is known that passivating groups such as –H and –OH species can be removed from diamond surfaces, thus allowing strong C–C bonds to form across the interface under vacuum or dry conditions. Exposure to humid air can rapidly replenish the passivating groups, which prevents C–C bond formation and maintains low friction and wear.[51,52] Under our atmospheric conditions, this will be strongly influenced by the presence of a capillary meniscus, which requires further study to understand fully.[53]

Pull-off forces were measured between the tips and a tetrahedral amorphous carbon (ta-C) sample[54] after every tenth AFM image (Figure 6b). ta-C is used as it has a very low roughness and thus leads to substantially less variability in the pull-off force measurements. The adhesive interactions between UNCD or $SiN_x$ tips and the ta-C sample can be quantified by using the Derjaguin–Muller–Toporov (DMT) model of contact mechanics,[55] which applies to weak, long-range adhesion between stiff materials. Modeling the AFM tip–sample interaction as a sphere contacting a flat plane, the DMT model relates the pull-off force $F$ to the work of adhesion $W$ and tip radius $R$:

$$F = 2\pi WR \quad (1)$$

If the surface chemistry between two materials remains constant during sliding, the work of adhesion will not vary and the pull-off force measurements therefore provide an indirect method for tracking changes in tip radius during wear experiments.[41] The DMT model used here is a continuum theory that provides a first-order approximation of the contact area and stresses. Recent atomistic simulations illustrate the potential complexity of the stress state at the tip–sample contact,[56,57] but nonetheless, application of the DMT formula consistently provides a useful comparison between the tips and insight into their evolution as they wear. Overall, the pull-off forces for the UNCD tips remain more consistent and lower than those measured for $SiN_x$ tips (Figure 6a), and follow the trends observed for tip radius (from both TEM and BTR) as a function of scan distance. In contrast to UNCD, both $SiN_x$ tips exhibit an increasing pull-off force throughout the tests, consistent with the substantial change in the geometry of the tips. From the measurements of tip radius and pull-off forces, the work of adhesion between the tips and sample surfaces are calculated using Equation (1) (Figure 6c). Overall, both $SiN_x$ and UNCD tips show relatively constant work of adhesion throughout the tests. There are some outlying points seen in Figure 6c, for example, at a distance of ~60 mm for the $SiN_x$ tip at 70% RH and a distance of ~120 mm for the $SiN_x$ tip at 15% RH, which correspond to sudden, transient changes in the work of adhesion (and correspondingly, in the surface chemistry) between the tips and the ta-C sample. This can occur due to localized contamination or attachment and detachment of nanoscale portions of the tip. It is also noticeable that the estimated work of adhesion for $SiN_x$ tips flattened under 70% RH becomes smaller from scan 101 to 200. This is most likely due to the deviation of the tip geometry (flat end) from the parabolic shape assumed in the DMT model [Eq. (1)].[58]

The volume loss of the UNCD and $SiN_x$ tips determined by TEM as a function of distance scanned is plotted in Figure 6d. Averaged over the entire period of scanning, the volumes

 © 2010 Wiley-VCH Verlag GmbH & Co. KGaA, Weinheim 

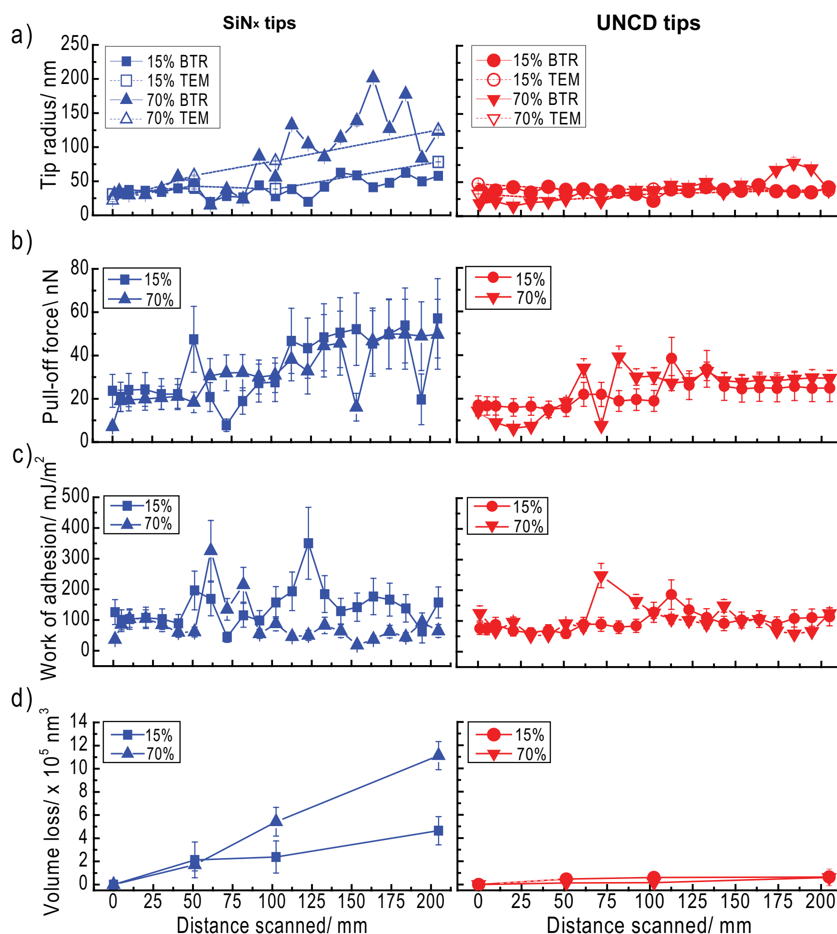


**Figure 6.** a) Tip radius of the UNCD and $SiN_x$ probes estimated from BTR and TEM measurement as a function of scan distance. b) Pull-off forces of UNCD and $SiN_x$ tips on ta-C surfaces as a function of distance scanned. c) Work of adhesion between a ta-C sample and the AFM tips as a function of scan distance. d) Comparison of wear volume loss versus distance scanned between the UNCD and $SiN_x$ tips under the different RH levels.

removed correspond to $180 \pm 47$ and $430 \pm 47$ atoms removed from the $SiN_x$ tip for every 1 μm line scanned at 15 and 70% RH, respectively, and $52 \pm 52$ and $55 \pm 17$ atoms removed from the UNCD tip for every 1 μm line scanned at 15 and 70% RH, respectively. The calculations assume an atomic density for UNCD and $SiN_x$ tips of $17.5 \times 10^{22}$ and $7.9 \times 10^{22}$ atom $cm^{-3}$, respectively.

Considering the delamination of the seed layer of the UNCD tip at 70% RH and the uncertainty in the wear volume measurement (estimated to be 0.001 $\mu m^3$ over ≈100 mm scanning distance based on the mismatch between the overlapped tip profiles and the resolution of the TEM images), it is possible that there was no net change in volume of the UNCD tip at 15% RH, or at 70% RH after the outer diamond seed layer was removed. The wear rates for $SiN_x$ tips were much higher than what has been observed by Gotsmann and Lantz[41] for Si tips, which was about one atom lost per micrometer scanning. This may be caused by several reasons: the polymeric sample in their study is much softer; the wear rates reduced as tip flattened at long scan distances (three orders of magnitude larger than our tests), significantly decreasing the average wear rate; and more direct, periodic characterization of the tip geometry in this paper enables better wear volume resolution.

A fuller appreciation of the wear resistance of UNCD probes can be achieved by calculating the contact radii and pressures experienced by the tip using DMT contact mechanics. The contact radius is given by:

$$a = \left(\frac{FR}{K}\right)^{1/3} \tag{2}$$

with $F$ the total load exerted on the tip, including applied load and adhesive force, and $K = \frac{4}{3}\left(\frac{1-\nu_1^2}{E_1} + \frac{1-\nu_2^2}{E_2}\right)^{-1}$, where $E_1$ and $E_2$ are the Young's moduli of the tip and substrate, respectively, and $\nu_1$ and $\nu_2$ are the Poisson's ratio of the tip and substrate, respectively.[59] The average contact pressure $P_{avg}$ is simply the applied force divided by the contact area:

$$P_{avg} = \frac{F}{\pi a^2} \tag{3}$$

The peak normal contact pressure is $P_{max} = 1.5\,P_{avg}$.

Due to the higher stiffness and lower work of adhesion of the UNCD tip, the DMT contact radius of UNCD tips is approximately two thirds of the $SiN_x$ contact radius, for the same tip radius, at zero externally applied load (0.9 versus 1.5 nm, respectively, averaged for each of the two tips at their initial radii). The smaller contact radius of UNCD indicates, in principle, smaller resolvable features of the tip. The average normal stress experienced by UNCD tips is therefore higher than that of $SiN_x$ tips by a factor of two, ≈7 GPa for UNCD and ≈3 GPa for $SiN_x$. Furthermore, as the $SiN_x$ tip is worn flat, the contact radius increases to the size of the tip, thus leading to decreased normal stress. Considering that frictional shear stress is proportional to the normal stress, the bulk UNCD tips exhibit little to zero measurable wear under a stress condition twice than that of $SiN_x$ tips, while $SiN_x$ tips shows significant, humidity-dependent wear.

## 3. Conclusions

Monolithic UNCD probes with integrated tips having small (30–40 nm) radii, smooth surfaces, and controlled geometry have been successfully fabricated by a wafer-level process. Comparisons between UNCD tips and commercial $SiN_x$ tips of similar geometry show that the UNCD tips have superior wear resistance to that of conventional $SiN_x$ tips under all conditions tested, which included low and high humidity, and stresses in the 2–8 GPa range scanned for 200 mm on a UNCD sample.


© 2010 Wiley-VCH Verlag GmbH & Co. KGaA, Weinheim

small

Wear is a complex phenomenon that depends on environment, sliding conditions, geometry, and the materials in contact. A wide range of these parameters must be studied to establish the generality of the promising wear performance of the UNCD tips observed here. However, these tests validate the conclusion that under the range of sliding conditions selected, UNCD probes provide improved wear resistance which is critically needed for advanced AFM applications, such as nanolithography, high-volume imaging, metrology, and nanomanufacturing.

## 4. Experimental Section

*Fabrication of UNCD AFM probes:* The fabrication procedure used to manufacture the UNCD probes is shown in Figure 7. Many elements of the process are similar to a procedure described elsewhere.[36] Starting substrates were (100) oriented 4'' silicon wafers with a 0.3-μm-thick thermal oxide layer. Square windows 8 μm in width were lithographically patterned into the oxide layer, and KOH orientation-dependent etching was used to generate pyramidal cavities with (111) sidewalls that served as molds for forming the diamond tips. Thermal oxidation at 950 °C was an optional step that could be used to sharpen the profile of the molds. A tungsten layer (≈50 nm in thickness), which enhanced the resulting diamond seeding procedure, was then sputter deposited. This layer was removed everywhere except from the pyramidal cavities by a self-aligned lithography step consisting of spin-coating photoresist, flood exposure, and developing, which left resist only in the cavities. After selectively etching the tungsten layer, the resist was treated and used as a mask to remove the $SiO_2$ layer from everywhere except the cavities.

Ultrasonic seeding with a solution of UDD nanoparticles provided the nucleation sites for diamond growth. UNCD was grown by HFCVD to a thickness of 1 μm. The diamond film was patterned to define the cantilevers by using a plasma-enhanced CVD (PECVD) $SiO_x$ layer as a hard mask and reactive ion etching (RIE) with an $O_2$–$CF_4$ plasma to etch the UNCD. The wafers were subsequently bonded to a partially prediced Pyrex 7740 substrate by using anodic bonding. After bonding, another dicing operation was used to define the glass chips. The probes were released from the mold by dissolving the Si wafers in KOH. The PECVD $SiO_x$ hard mask was then removed by a buffered oxide etch (BOE). Residual tungsten and tungsten carbide were cleaned from the tips by etching in hydrogen peroxide and potassium ferricyanide/KOH/water (Murakami) solutions, respectively. A final cleaning step with piranha solution and a deionized water rinse was performed to remove any other remaining contaminants.

*Wear characterization methodology:* The protocol for the wear tests involved the following steps. Optical microscopy and white-light interferometry (Zygo NewView) were employed to measure the in-plane dimensions and curvature, respectively, of the fabricated UNCD probes. Cantilever thickness, tip morphology, and tip radius were evaluated by SEM (FEI Nova) and TEM (JEOL 200CX-II and JEOL 2010F). The radii of the tips were determined from the TEM images through the use of a custom Matlab script, which allowed for tracing the two-dimensional profile of each tip,

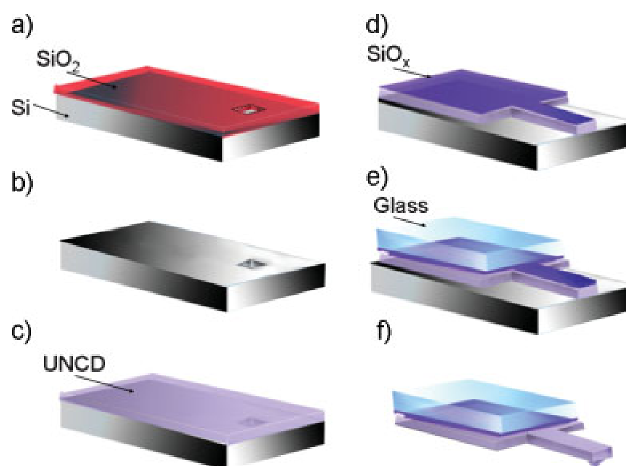


Figure 7. Wafer-level microfabrication process to manufacture UNCD AFM probes. a) A thermal oxide ($SiO_2$) is grown on the wafer, followed by photolithography and buffered oxide etch (BOE) to create a hard mask for etching the pyramidal cavities. b) Anisotropic KOH etching of Si is used to form pyramidal cavities that serve as molds for the tips. The $SiO_2$ is stripped, and oxidation sharpening of the molds is performed (optional). c) Tungsten is sputter deposited on the surface followed by seeding and UNCD deposition by HFCVD. d) The UNCD layer is patterned to form the cantilevers using a PECVD $SiO_x$ hard mask and RIE etching of the UNCD. e) The wafer is bonded to a partially diced glass handle wafer by anodic bonding. f) Final release of the cantilevers is performed by KOH etching of the Si mold wafer, and removal of the hard mask oxide by BOE. Additional details are provided in the text.

and fitting the tip apex with a parabola using a least-squares algorithm to determine the tip radius. The normal spring constants $k$ of the cantilevers were calculated by using the in-plane cantilever dimensions, the thickness, and the elastic modulus of the lever material.[60] Young's modulus values of 900 ± 100 GPa for UNCD[61] and 180 ± 20 GPa for $SiN_x$[62] were assumed in all calculations.

Wear tests were performed by scanning tips against a UNCD substrate. UNCD was chosen as a substrate due to its high hardness and a consistent nanoscale roughness that allowed assessment of the nanoscale imaging performance by using BTR. The tests consisted of acquiring a series of 200 $1 \times 1\ \mu m^2$ contact-mode AFM images with 512 lines per scan. The 200 scans were periodically interrupted to characterize the tip geometry by TEM and adhesion measurements. During acquisition of a single $1 \times 1\ \mu m^2$ AFM image (trace and retrace), the tip nominally traveled 1.024 mm per image. Based on calibration performed before and after the measurements, we estimated a systematic error of no more than ±5% in scan distance due to uncertainty in the calibration of the piezoelectric scanner. A small number of additional scan lines were traversed each time the tip was reengaged with the sample; thus, there was an additional uncertainty of up to 0.02 mm over every ten images (10.3 mm). The scanning speed was varied over the course of the test: the speed was increased from 3.75 to 17.4 $\mu m\ s^{-1}$ at ≈3 $\mu m\ s^{-1}$ increments every 20 images for the first 100 images, and was 20.3 $\mu m\ s^{-1}$ from images 101 to 200. During the first 100 images, the tip was loaded by adhesive forces alone (zero externally applied load). From image 101 to 200, an external load equal to twice that of the adhesive pull-off force between the tip and a ta-C

 © 2010 Wiley-VCH Verlag GmbH & Co. KGaA, Weinheim 

sample was used. The humidity was measured with a hygrometer and kept at the desired value by controlling the flow of dry nitrogen through a deionized-water bath into an environmental chamber surrounding the AFM instrument. The wear tests were conducted at two different humidity levels: 15 and 70% RH.

Surface topography images obtained at each scan were used to deduce the tip radius by BTR, a process based on convolution/deconvolution theory,[46] by using the scanning probe image processor (SPIP) software program. Careful selection of the parameters that control the reconstruction algorithm was essential for producing reliable and consistent results and will be described in detail elsewhere.[63] Briefly, the reconstructed tip shape represents an upper bound, that is, the largest possible tip that could have produced the topographic images. The AFM images of UNCD surfaces were flattened and Fourier-filtered to eliminate any spatial frequency that was higher than the scan resolution ($\approx$2 nm). The reconstruction parameters chosen were: reconstruction size $27 \times 27$ pixels, ignore lower values of 30%, three iterations, and an acceptance level of 5–10. The obtained BTR tip profiles along the $y$ direction were rotated by 11° (tilt angle of the AFM chip holder) and overlapped with tip profiles from TEM measurement at the point of the tip apex. Considering the positioning of cantilevers in AFM and TEM, the overlay the tip profiles obtained by the TEM and BTR techniques shows very good agreement.

After every ten image scans, the pull-off deflection $\delta$ was measured at five different positions on the ta-C sample to determine the tip–sample pull-off force $F = k\delta$. Since ta-C has a surface roughness of <0.8 nm and is composed of up to 80% $sp^3$-bonded carbon, it provides a flat, stiff test surface with a surface energy comparable to that of UNCD. The error bars shown for the adhesion measurements reflect the standard error in the measurements and uncertainties in the experimentally calibrated cantilever stiffness. The evolution in tip morphology and radius was characterized by TEM immediately after images 0, 50, 100, and 200 were acquired. A detailed description of the wear characterization methodology will be presented elsewhere.[63]

### Acknowledgements

*We thank Guoqing Ning and S. S. Sudheer for assistance with developing microfabrication processes and Ralu Divan for assistance in process development. We thank Jennifer Gerbi and James Birrell for useful discussions and assistance with developing UNCD deposition methodologies. We thank Orlando Auciello for useful discussions and guidance. Advanced Diamond Technologies, the University of Wisconsin–Madison, and the University of Pennsylvania acknowledge support under NSF STTR Grants #0638030 and #0823002. R.W.C. acknowledges support from the National Science Foundation, grant number CMMI-0826076, and the Nano/Bio Interface Center at the University of Pennsylvania through the National Science Foundation NSEC DMR-0425780. K.T.T. and J.L. acknowledge the National Science Foundation for support under CMMI grant #0825000 and facilities support under DMR #0520527. The work at Argonne National Laboratory was supported by the US Department of Energy, Office of Science, Office of Basic Energy Sciences, under Contract No. DE-AC02-06CH11357. Note: J.A.C. and N.M. have a competing financial interest. This work was primarily supported by a NSF STTR (Small Business Technology Transfer) grant led by Advanced Diamond Technologies, Inc. (ADT). The diamond AFM probes studied herein were developed under this project and are now being sold by ADT through its own website and through various distributors to AFM users around the world. N.N. no longer works at ADT.*

[1] F. J. Giessibl, *Science* **1995**, *267*, 68–71.
[2] A. Yacoot, L. Koenders, *J. Phys. D: Appl. Phys.* **2008**, *41*, 103001.
[3] X. N. Xie, H. J. Chung, C. H. Sow, A. T. S. Wee, *Mater. Sci. Eng. R* **2006**, *54*, 1–48.
[4] R. D. Piner, J. Zhu, F. Xu, S. Hong, C. A. Mirkin, *Science* **1999**, *283*, 661–663.
[5] P. Vettiger, G. Cross, M. Despont, U. Drechsler, U. Durig, B. Gotsmann, W. Haberle, M. A. Lantz, H. E. Rothuizen, R. Stutz, G. K. Binnig, *IEEE Trans. Nanotechnol.* **2002**, *1*, 39–54.
[6] A. G. Khurshudov, K. Kato, H. Koide, *Tribol. Lett.* **1996**, *2*, 345–354.
[7] M. L. Bloo, H. Haitjema, W. O. Pril, *Measurement* **1999**, *25*, 203–211.
[8] Q. L. Zhao, S. Dong, T. Sun, *Key Eng. Mater.* **2001**, *202–203*, 315–320.
[9] W. Maw, F. Stevens, S. C. Langford, J. T. Dickinson, *J. Appl. Phys.* **2002**, *92*, 5103–5110.
[10] M. D'Acunto, *Nanotechnology* **2004**, *15*, 795–801.
[11] K.-H. Chung, Y.-H. Lee, D.-E. Kim, *Ultramicroscopy* **2005**, *102*, 161–171.
[12] H. Liu, M. Klonowski, D. Kneeburg, G. Dahlen, M. Osborn, T. Bao, *J. Vac. Sci. Technol. B* **2005**, *23*, 3090–3093.
[13] Z. Tao, B. Bhushan, *Tribol. Lett.* **2006**, *21*, 1–16.
[14] H. Bhaskaran, A. Sebastian, M. Despont, *IEEE Trans. Nanotechnol.* **2009**, *8*, 128–131.
[15] M. Kopycinska-Mueller, R. H. Geiss, D. C. Hurley, *Mater. Res. Soc. Symp. Proc.* **2006**, *924*, 19–24.
[16] T. R. Albrecht, S. Akamine, T. E. Carver, C. F. Quate, *J. Vac. Sci. Technol. A* **1990**, *8*, 3386–3396.
[17] H. J. Dai, J. H. Hafner, A. G. Rinzler, D. T. Colbert, R. E. Smalley, *Nature* **1996**, *384*, 147–150.
[18] N. R. Wilson, J. V. Macpherson, *Nat. Nanotechnol.* **2009**, *4*, 483–491.
[19] E. Rabinowicz, *Friction and Wear of Materials*, 2nd ed. Wiley, New York **1995**.
[20] H. P. Jost, *Tribol. Lubr. Technol.* **2005**, *61*, 18–22.
[21] K. E. Petersen, *Proc. IEEE* **1982**, *70*, 420–457.
[22] R. Maboudian, *Surf. Sci. Rep.* **1998**, *30*, 207–269.
[23] K.-H. Chung, Y.-H. Lee, D.-E. Kim, *Ultramicroscopy* **2005**, *102*, 161–171.
[24] K.-H. Chung, D.-E. Kim, *Tribol. Lett.* **2003**, *15*, 135–144.
[25] A. L. Ruoff, *J. Appl. Phys.* **1979**, *50*, 3354–3356.
[26] A. Nesmelov, *Diamond Tools in Industry*, Mashinostroeniye, Moscow **1964**.
[27] O. Lysenko, N. Novikov, V. Grushko, A. Shcherbakov, A. Katrusha, S. Ivakhnenko, V. Tkach, A. Gontar, *Diamond Relat. Mater.* **2008**, *17*, 1316–1319.
[28] B. Mesa, S. Magonov, *J. Phys. Conf. Ser.* **2007**, *61*, 770–774.
[29] C. T. Gibson, S. Carnally, C. J. Roberts, *Ultramicroscopy* **2007**, *107*, 1118–1122.
[30] T. Larsen, K. Moloni, F. Flack, M. A. Eriksson, M. G. Lagally, C. T. Black, *Appl. Phys. Lett.* **2002**, *80*, 1996–1998.


© 2010 Wiley-VCH Verlag GmbH & Co. KGaA, Weinheim

[31] D. Álvarez, M. Fouchier, J. Kretz, J. Hartwich, S. Schoemann, W. Vandervorst, *Microelectron. Eng.* **2004**, *73-74*, 910–915.
[32] K.-H. Chung, D.-E. Kim, *Ultramicroscopy* **2007**, *108*, 1–10.
[33] P. Niedermann, W. Hänni, D. Morel, A. Perret, N. Skinner, P.-F. Indermühle, N.-F. de Rooij, P.-A. Buffat, *Appl. Phys. A* **1998**, *66*, S31–S34.
[34] A. Kant, M. D. Drory, N. R. Moody, W. J. Moberly Chan, J. W. Ager, R. O. Ritchie, *Mater. Res. Soc. Symp. Proc.* **1998**, *505*, 611–616.
[35] O. Auciello, J. Birrell, J. A. Carlisle, J. E. Gerbi, X. Xiao, B. Peng, H. D. Espinosa, *J. Phys.: Condens. Matter* **2004**, *16*, 539–552.
[36] K.-H. Kim, N. Moldovan, C. Ke, H. D. Espinosa, X. Xiao, J. A. Carlisle, O. Auciello, *Small* **2005**, *1*, 866–874.
[37] K. H. Kim, N. Moldovan, C. Ke, H. D. Espinosa, X. Xiao, J. A. Carlisle, O. Auciello, *Small* **2005**, *1*, 912.
[38] M. Ozawa, M. Inaguma, M. Takahashi, F. Kataoka, A. Kruger, E. Osawa, *Adv. Mater.* **2007**, *19*, 1201–1206.
[39] N. N. Naguib, J. W. Elam, J. Birrell, J. Wang, D. S. Grierson, B. Kabius, J. M. Hiller, A. V. Sumant, R. W. Carpick, O. Auciello, J. A. Carlisle, *Chem. Phys. Lett.* **2006**, *430*, 345–350.
[40] M. D'Acunto, *Nanotechnology* **2006**, *17*, 2954–2962.
[41] B. Gotsmann, M. A. Lantz, *Phys. Rev. Lett.* **2008**, *101*, 125501.
[42] F. Katsuki, A. Saguchi, W. Takahashi, J. Watanabe, *Jpn. J. Appl. Phys.* **2002**, *41*, 4919–4923.
[43] J. T. Dickinson, *J. Chem. Educ.* **2005**, *82*, 734–742.
[44] S. Kopta, M. Salmeron, *J. Chem. Phys.* **2000**, *113*, 8249–8252.
[45] N. M. Pugno, R. Agrawal, H. D. Espinosa, *Rev. Adv. Mater. Sci.* **2009**, *19*, 73–77.
[46] J. S. Villarrubia, *J. Res. Natl. Inst. Stand. Technol.* **1997**, *102*, 425.
[47] M. Chen, K. Kato, K. Adachi, *Wear* **2001**, *250*, 246–255.
[48] S. Jahanmir, T. E. Fischer, *Tribol. Trans.* **1988**, *31*, 32–43.
[49] V. A. Muratov, T. Luangvaranunt, T. E. Fischer, *Tribol. Int.* **1998**, *31*, 601–611.
[50] R. Agrawal, N. Moldovan, H. D. Espinosa, *J. Appl. Phys.* **2009**, *106*, 064311.
[51] Q. Yue, E. Konca, A. T. Alpas, *Surf. Sci.* **2006**, *600*, 2955–2965.
[52] A. R. Konicek, D. S. Grierson, P. U. P. A. Gilbert, W. G. Sawyer, A. V. Sumant, R. W. Carpick, *Phys. Rev. Lett.* **2008**, *100*, 235502.
[53] R. W. Carpick, J. Batteas, M. Boer, *Scanning Probe Studies of Nanoscale Adhesion Between Solids in the Presence of Liquids and Monolayer Films* (Ed.: B. Bhushan), Springer, Berlin **2007**.
[54] T. A. Friedmann, J. P. Sullivan, J. A. Knapp, D. R. Tallant, D. M. Follstaedt, D. L. Medlin, P. B. Mirkarimi, *Appl. Phys. Lett.* **1997**, *71*, 3820–3822.
[55] B. V. Derjaguin, V. M. Muller, Y. P. Toporov, *J. Colloid Interface Sci.* **1975**, *53*, 314–326.
[56] B. Luan, M. O. Robbins, *Nature* **2005**, *435*, 929–932.
[57] Y. Mo, K. T. Turner, I. Szlufarska, *Nature* **2009**, *457*, 1116–1119.
[58] T. Tian, H. Chung-Yuen, *J. Polym. Sci. Polym. Phys.* **2005**, *43*, 3628–3637.
[59] K. L. Johnson, *Contact Mechanics*, Cambridge University Press, Cambridge **1987**.
[60] C. A. Clifford, M. P. Seah, *Nanotechnology* **2005**, *16*, 1666–1680.
[61] H. D. Espinosa, B. C. Prorok, B. Peng, K. H. Kim, N. Moldovan, O. Auciello, J. A. Carlisle, D. M. Gruen, D. C. Mancini, *Exp. Mech.* **2003**, *43*, 256–268.
[62] R. A. Levy, X. Lin, J. M. Grow, H. J. Boeglin, R. Shalvoy, *J. Mater. Res.* **1996**, *11*, 1483–1488.
[63] J. Liu, J. Notbohm, K. T. Turner, R. W. Carpick, unpublished results.
[64] A. R. Krauss, O. Auciello, D. M. Gruen, A. Jayatissa, A. Sumant, J. Tucek, D. C. Mancini, N. Moldovan, A. Erdemir, D. Ersoy, M. N. Gardos, H. G. Busmann, E. M. Meyer, M. Q. Ding, *Diamond Relat. Mater.* **2001**, *10*, 1952–1961.
[65] R. G. José, S. M. Antônio, F. S. Rui, M. V. Joaquim, *J. Am. Ceram. Soc.* **1999**, *82*, 953–960.

Received: September 6, 2009
Revised: March 7, 2010


© 2010 Wiley-VCH Verlag GmbH & Co. KGaA, Weinheim